molecules

MDPI

Article

Adsorption of O_2 on the Preferred -O-Au Sites of Small Gold Oxide Clusters: Charge-dependent Interaction and Activation

Lulu Huang, Wen Liu and Xiaopeng Xing *

Shanghai Key Lab of Chemical Assessment and Sustainability, Department of Chemistry, Tongji University, 1239 Siping Road, Shanghai 200092, China; huanglulu@tongji.edu.cn (L.H.); 2410277@tongji.edu.cn (W.L.)
* Correspondence: xingxp@tongji.edu.cn

Abstract: Decades of research have illuminated the significant roles of gold/gold oxide clusters in small molecule catalytic oxidation. However, many fundamental questions, such as the actual sites to adsorb and activate O_2 and the impact of charge, remain unanswered. Here, we have utilized an improved genetic algorithm program coupled with the DFT method to systematically search for the structures of $Au_{1-5}O_x^{-/+/0}$ (x = 1–4) and calculated binding interactions between $Au_{1-5}O_x^{-/+/0}$ (x = 1–2) and O_2, aiming to determine the active sites and to elucidate the impact of different charge states in gold oxide systems. The results revealed that the reactivity of all three kinds of small gold oxide clusters toward O_2 is strongly site-dependent, with clusters featuring an -O-Au site exhibiting a preference for adsorption. The charges on small gold oxide clusters significantly impact the interaction strength and the activation degree of adsorbed O_2: in the case of anionic cluster, the interaction between O_2 and the -O-Au sites leads to a chemical reaction involving electron transfer, thereby significantly activating O_2; in neutral and cationic clusters, the adsorption of O_2 on their -O-Au sites can be viewed as an electrostatic interaction. Pointedly, for cationic clusters, the highly concentrated positive charge on the Au atom of the -O-Au sites can strongly adsorb but hardly activate the adsorbed O_2. These results have certain reference points for understanding the gold oxide interfaces and the improved catalytic oxidation performance of gold-based systems in the presence of atomic oxygen species.

Keywords: gold oxide clusters; charge-dependence; oxygen activation; active sites

Citation: Huang, L.; Liu, W.; Xing, X. Adsorption of O_2 on the Preferred -O-Au Sites of Small Gold Oxide Clusters: Charge-dependent Interaction and Activation. *Molecules* **2024**, *29*, 1645. https://doi.org/10.3390/molecules29071645

Academic Editor: Erich A. Müller

Received: 12 March 2024
Revised: 1 April 2024
Accepted: 4 April 2024
Published: 6 April 2024

1. Introduction

Catalysis plays a substantial role in agricultural, industrial, and environmental fields, serving as one of the pivotal topics within the scope of chemical research. Notably, metallic nanocatalysts loaded on various oxides represent one of the most common forms of catalysts [1–6]. Gold, perceived as an exceedingly inert metal since ancient times, was discovered, by Haruta [7–9] and Hutchings [10,11] at the end of the last century, to exhibit remarkable catalytic oxidation activity toward CO and other small organic molecules. This groundbreaking discovery precipitated a surge in the amount of research related to gold systems, gradually culminating in the establishment of an independent field of study.

Decades of research have illuminated the significant roles of gold nanoparticles, gold clusters, and even a single gold atom in small molecule catalytic oxidation [12–17]. However, many fundamental questions, such as the location of O_2 adsorption and activation [12,18–22] and the impact of charge [3,20,23–32], still remain contested. Some studies suggest that the presence of gold at the oxide interface and gold oxides are key to O_2 activation, and the introduction of these elements can improve the catalytic oxidation performance of these systems [32–39]. However, there is still a lack of detailed explanation at the atomic and molecular levels for specific sites and their mechanisms. In addition, researchers have found that gold clusters carrying either positive or negative charges both demonstrated catalytic activity in specific systems [23,26–33]. This suggests that various

active sites with different charge states and spatial geometrical conditions might be involved in real catalytic processes [40]. In experiments, X-ray photoelectron spectroscopy is commonly utilized to assess charge transfer among nanomaterials. Nonetheless, conducting spectral analysis at such small scales poses a significant challenge and can even yield misleading results [3,41].

By adopting the cluster model which boasts advantages such as controllable preparation, simplicity, and close linkage with DFT theoretical computations, we can comprehend the mechanisms of heterogeneous catalysis interacting with small molecules at the atomic and molecular level [42–45]. Insights into the activation of O_2 on gold-based catalysts have been derived from comprehensive studies on the reactions between various gold clusters and O_2, merging data from numerous experiments and calculations [18,20,46–55]. Consistent findings indicate O_2 functioning as a one-electron acceptor during its interactions with gold clusters, with electron transfer from gold to its anti-bonding π^*_{2p} enhancing its adsorption and activation. The strong chemical interactions with O_2 are primarily due to the unpaired electrons and the low electron binding energy inherent to gold clusters. Theoretical explorations have also been conducted on gold clusters containing one or two O atoms [53,55,56]. These O atoms tend to occupy terminal positions in clusters comprising no more than three gold atoms, or they bridge two peripheral gold atoms [56]. It has been generally observed that gold clusters featuring two separate O atoms maintain greater stability than their counterparts which adsorb an O_2 molecule, particularly when the clusters incorporate more than three gold atoms [51,53,55]. Furthermore, some small gold oxide clusters, specifically $AuO_{1\text{-}2}^-$ and $Au_{2,4}O_2^-$, have been generated within the plasma of the laser-vaporization cluster source. Combinatorial analysis using photoelectron spectrometry experiments and calculations determined their structures [52,57]. The interactions between $Au_xO_y^{+/-}$ and CO have been thoroughly examined using a flow tube reactor, which illuminated several reaction channels [58–62]. We previously explored reactivity of AuO_x^- (x = 1–3) with O_2 and found that only AuO^- is active [63]. Recently, we have indicated that -O-Au is the preferred adsorption site for O_2 on small anionic gold oxide clusters through theoretical calculations and mass spectrometry experiments, and the correlation with the global electronic characteristics is insignificant [64].

Compared with common cluster models, actual heterogeneous catalytic sites tend to be neutral or carry a small amount of charge due to charge transfer [30,65]. Therefore, revealing the relationships between cluster reactivity and the polarity and amount of charge on the clusters is crucial to scrutinize reaction mechanisms on actual catalysts based on cluster reaction results. This study aims to elucidate the impact of different charge states of gold oxide systems on O_2 adsorption and activation, which is the rate-limiting step in many catalytic oxidation processes [32,66–68]. In this paper, we have carried out extensive theoretical calculations on the structures of $Au_{1–5}O_{1,2}^{-/+/0}$ and the adsorption and activation of O_2 on them. The results indicate that, no matter what the charge state of the cluster is, the -O-Au site is the preferred adsorption site for O_2, with the largest binding energy. However, due to the different valence bond interactions formed on clusters' various charge states, only the -O-Au sites in the anionic gold oxide clusters can significantly activate O_2.

2. Results and Discussion

2.1. Geometric Structures of $Au_{1–5}O_{1,2}^-$ and Their Products with an O_2

The low-lying structures of $Au_{1–5}O_{1,2}^-$ have been reported in our previous work [64], and Figure 1 shows the lowest-lying ones. For references to other low-lying structures, please refer to Figures S1–S4 in the Supplementary Materials. In Figure 1, the O atoms in $Au_{1–5}O^-$ are coordinated to one or two Au atoms, which is consistent with previous results [56]; for $Au_{1–5}O_2^-$, when the number of Au atoms is odd, the energy of the oxide formation is energetically favorable (with O atoms dissociated), whereas when the number of Au atoms is even, the formation with an absorbed O_2 becomes the most energetically

favorable structure. The most energetically advantageous adsorption site for the O_2 in $Au_{2,4}O_2^-$ is consistent with previous theoretical results [49–51,55,69,70].

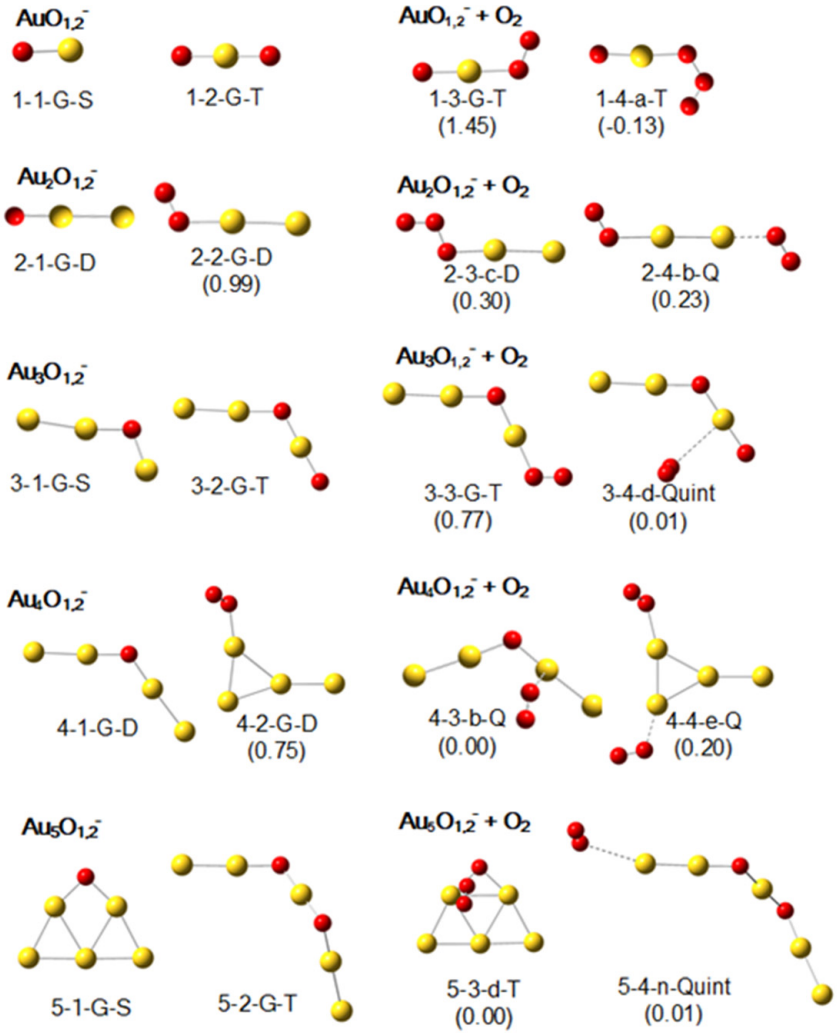

Figure 1. The lowest-lying structures of $Au_{1-5}O_x^-$ (x = 1 and 2) and their most stable products after adsorbing one O_2 according to calculations at the B3LYP level with the basis sets of def2-SVP for Au, and def2-TZVP for O. In the labels of the structures, the first two numerals indicate the number of gold atoms and the number of oxygen atoms, respectively; the third part "G/a/b…" means that this structure is the lowest-lying, the second lowest-lying, or the third lowest-lying one among all structural candidates; the fourth part indicates the spin-multiplicity, in which "S", "D", "T", "Q", and "Quint" stand for singlet, doublet, triplet, quartet, and quintet, respectively. The numerals in the parentheses following the labels of the structures containing adsorbed O_2 unit(s) show the adsorption energies (E_a, in eV) of the second O_2.

For the structures of $Au_{1-5}O_{1,2}^-$, illustrated in the left two columns of Figure 1, only 1-1-G-S and 3-1-G-S have an -O-Au site, and adsorption of O_2 on these two structures forms 1-3-G-T and 3-3-G-T with the largest two adsorption energies of 1.45 eV and 0.77 eV, respectively (in the right two columns of Figure 1). Similar situations can also be repeatedly confirmed in the Supplementary Materials, such as the O_2 adsorption products of 1-4-G-T (E_a: 1.05 eV), 2-3-b-D (E_a: 1.35 eV), and 2-4-G-D (E_a: 1.05 eV) in Figure S1. Also, for clusters with a slightly larger number of gold atoms in Figures S2–S4, we can find 3-4-b-T (E_a: 1.15 eV), 3-4-c-T (E_a: 0.87 eV), and 5-4-g-T (E_a: 0.89 eV) and many other structures that comply with the adsorption rules. Namely, if the -O-Au site is present, the adsorption energy of O_2 on it is the largest (approx. 0.5–1.5 eV). However, if there is no such site, the

adsorption of O_2 is extremely weak, as demonstrated by 3-4-d-Quint (E_a: 0.01 eV), 4-3-b-Q (E_a: 0.00 eV), and 5-4-n-Quint (E_a: 0.01 eV) in Figure 1. Additional examples for this weak interaction can be found in the Supplementary Materials (Figures S1–S4).

2.2. Geometric Structures of $Au_{1-5}O_{1,2}^+$ and Their Products with an O_2

The lowest-lying structures of $Au_{1-5}O_{1,2}^+$ are shown in the left two columns of Figure 2. In the geometric structures of $Au_{2-5}O^+$, the O atom connects three gold atoms when the number of Au atoms is odd, and it connects two gold atoms when the number of Au atoms is even. Our computational work remains consistent with previous work [56]. For $Au_{1-5}O_2^+$, the lowest-lying structures can be interpreted as the lowest-lying cationic pure gold cluster adsorbed an O_2 [71–73]. The adsorption energies of O_2 clearly show that, with the exception of AuO_2^+ (E_a: 0.50 eV), the adsorption interaction here is relatively low, which is consistent with the results of Ding et al. [70]. Additionally, there is a decreasing trend in adsorption energies as the number of gold atoms increases, which may be related to what we will discuss later: for cationic gold oxide clusters and neutral gold oxide clusters, the adsorption energy of O_2 on them is proportional to the amount of positive charge on the Au atom of the -O-Au sites.

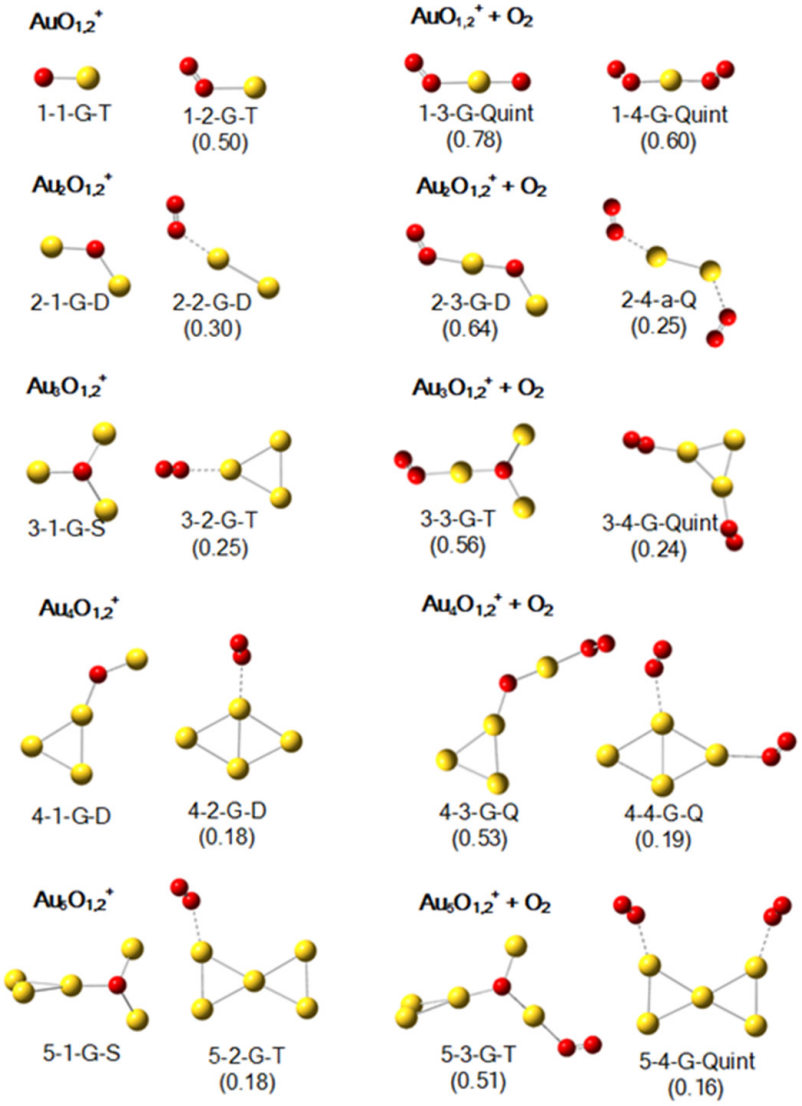

Figure 2. The lowest-lying structures of $Au_{1-5}O_x^+$ (x = 1 and 2) and their most stable products after adsorbing one O_2 according to calculations at the B3LYP level with the basis sets of def2-SVP for Au, and def2-TZVP for O. The meanings of the labels and the numerals are the same as those in Figure 1.

As shown in the right two columns of Figure 2, the adsorption energies of O_2 on the -O-Au sites of 1-1-G-T and 2-1-G-D remain high, at approximately 0.78 eV (1-3-G-Quint) and 0.64 eV (2-3-G-D), respectively. The adsorption energies of O_2 on the -O-Au sites of 3-1-G-S, 4-1-G-D and 5-1-G-S are 0.56 eV (3-3-G-T), 0.53 eV (4-3-G-Q), and 0.51 eV (5-3-G-T), respectively. This observed preference is similar to our prior findings regarding anionic gold oxide clusters [64]. Apart from the ones shown in Figure 2, Figures S5–S8 in the Supplementary Materials provide other examples to repeatedly confirm this preference (such as the adsorbed O_2 in 2-4-G-Q, 2-4-c-D, 3-3-b-Quint, 3-4-a-Quint and 5-4-a-Quint). In a word, the adsorption energy of O_2 on the -O-Au site is higher than that on other sites, with the majority of clusters' adsorption energies around 0.5 eV.

In the absence of the -O-Au site, the adsorption will be weak. As portrayed in Figure 2, the structures 2-4-a-Q, 3-4-G-Quint, 4-4-G-Q, and 5-4-G-Quint exhibit adsorption energies of merely 0.25 eV, 0.24 eV, 0.19 eV, and 0.16 eV, respectively. In Figure 2, the $Au_{1-5}O_4^+$ clusters can be regarded as pure gold clusters adsorbing two molecular oxygen. The values of adsorption energies in this study align well with those reported by Ding et al., with only minor discrepancies observed in the adsorption sites of 4-4-G-Q and 5-4-G-Quint [70]. As shown in Figure S6, the 3-2-b-T encompasses both an -O-Au site and an -O-Au-Au site, and the adsorption energy at the active site is 0.51 eV (3-4-b-Quint), whereas that on the -O-Au-Au site is only 0.10 eV (3-4-c-Quint). In Figure S7, 4-1-b-D has a gold triangle and an -O-Au site, and the adsorption energy of O_2 on its gold triangle and -O-Au site is calculated to be 0.17 eV (4-3-g-D) and 0.50 eV (4-3-d-Q), respectively. An analogous weak adsorption scenario can be observed in many other adsorption structures like 3-3-g-Quint, 5-3-a-T, and 5-4-c-Quint in Figures S6 and S8.

2.3. Geometric Structures of $Au_{1-5}O_{1,2}^0$ and Their Products with an O_2

The lowest-lying structures of $Au_{1-5}O_{1,2}$ are shown in the left two columns of Figure 3. For the clusters with one or three gold atoms, the O is mono-coordinated, whereas when the number of gold atoms is equal to 2, 4, or 5, the O atom is di-coordinated. The lowest-lying structures obtained by our calculations are consistent with previously reported results [56]. For $Au_{1-5}O_2$, the lowest-lying structures are those with molecular oxygen adsorbed onto pure gold clusters. It is noteworthy that when the number of gold atoms is three or five, peroxide adsorption forms, with adsorption energies of 0.49 eV and 0.64 eV being found. These two peroxide structures are consistent with previous results [70], and their O_2 units are highly activated: the O-O bond length, O-O vibration frequency, and NPA charge on O_2 are 1.281 Å, 1199.00 cm^{-1}, and −0.427 a.u. for Au_3O_2, and 1.316 Å, 1161.80 cm^{-1}, and −0.540 a. u. for Au_5O_2.

As shown in the right two columns of Figure 3, the corresponding adsorption structures of 1-1-G-D, 2-1-G-S, and 4-1-G-S are 1-3-G-Q, 2-3-G-T, and 4-3-a-T, respectively. The original structures all have active -O-Au sites, and the adsorption energies of O_2 on these sites are 0.39 eV, 0.38 eV, and 0.36 eV, respectively. Aside from those shown in Figure 3, there are other examples in the Supplementary Materials. As can be seen in Figure S9, the corresponding adsorption structure of 2-2-a-T is 2-4-b-Quint, and the adsorption energy on its -O-Au site is 0.40 eV. Some additional examples include 3-4-b-Q and 3-4-e-Q from Figure S10; 4-3-e-T, 4-3-h-T and 4-4-j-Quint from Figure S11; and 5-4-i-Q from Figure S12. In a word, if there is an -O-Au site, the adsorption energy of O_2 is maximal (relative to other sites), and the adsorption energies on these sites are typically slightly less than 0.4 eV.

If there is no -O-Au site, adsorption of O_2 is extremely weak. As depicted in Figure 3, the corresponding adsorption structures of 3-1-G-D and 5-1-G-D are 3-3-a-Q and 5-3-c-Q with the adsorption energies of 0.10 eV and 0.01 eV, respectively. There are other examples in the Supplementary Materials (Figures S9–S12), which are not all enumerated. The adsorption energies of the second O_2 on $Au_{1-5}O_2$ are nearly identical to the previous theoretical results predicted by Ding et al. [70].

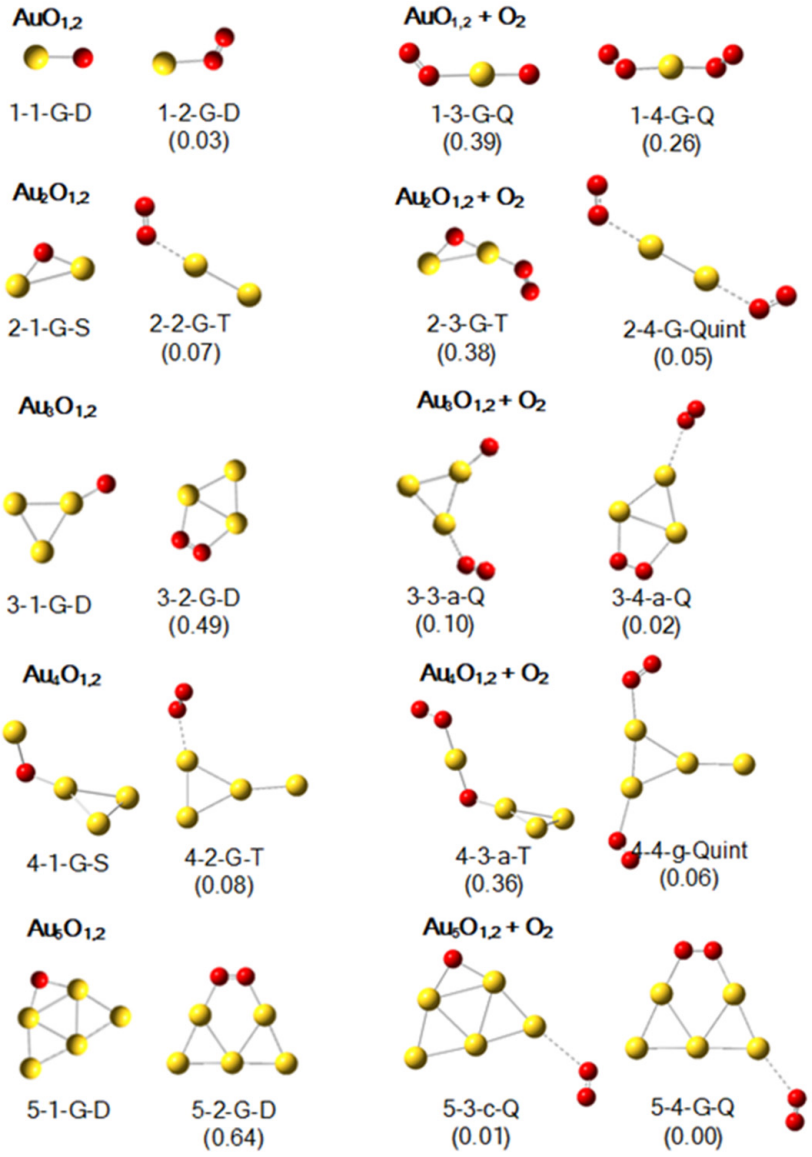

Figure 3. The lowest-lying structures of $Au_{1–5}O_x$ (x = 1 and 2) and their most stable products after adsorbing one O_2 according to calculations at the B3LYP level with the basis sets of def2-SVP for Au, and def2-TZVP for O. The meaning of the labels and the numerals are same as those in Figure 1.

2.4. Charge-Dependent Bonding Strengths and Activation Degrees

To summarize and compare the adsorption energies and the activation degree of O_2 on the -O-Au sites in the structures depicted in Figures 1–3, we present related calculated parameters of the adsorbed O_2 in Table 1. Anionic gold oxide clusters exhibit the largest binding energies for O_2 among the three series, along with the longest O-O bond lengths (above 1.32 Å). The calculated bond length of a free O_2 stands at 1.204 Å (1.208 Å as reported in an experiment by [74]), so anionic gold oxide clusters show a significant stretching of the O-O bond. Simultaneously, the O_2 units on anionic gold oxide clusters accumulate more than 0.6 a.u. negative charges, and their spins are close to 1.0. All these parameters indicate that the adsorbed O_2 on the -O-Au sites of these anionic gold oxide clusters gain an electron onto its π^* anti-bonding orbital, which significantly activates the O-O bond. For cationic gold oxide clusters, apart from 1-3-G-Quint and 2-3-G-D, which have adsorption energies of 0.78 eV and 0.64 eV, respectively, the rest of the structures tend to have adsorption energies slightly higher than 0.50 eV. The O-O bond lengths of the adsorbed O_2 on these cationic gold oxide clusters are around 1.21 Å, which is very close to that of a free O_2; the adsorbed

O_2 units are slightly positively charged, and their spins are close to that of free O_2. All these parameters indicate that the O_2 units on the -O-Au sites of the cationic gold oxide clusters are almost not activated. Neutral gold oxide clusters show adsorption energies slightly lower than 0.4 eV, with corresponding O-O bond lengths distributed around 1.225 Å, which is between those of the aforementioned anionic and cationic ones. Their O_2 units carry a slight negative charge. Compared to free O_2, the spins of the adsorbed O_2 on these neutral gold oxide clusters decrease a little, implying the weak activation of O_2 on the neutral species despite its relatively weak binding.

Table 1. The adsorption energies (E_a), the bond lengths ($BL_{O\text{-}O}$), the NPA charges ($Charge_{O\text{-}O}$), and the spins ($Spin_{O\text{-}O}$) of the O_2 units adsorbed on the -O-Au sites of the $Au_nO^{-/+/0}$ shown in Figures 1–3.

$Au_nO^{-/+/0}$ + O_2 Corresponding Pro		E_a (eV)	$BL_{O\text{-}O}$ (Å)	$Charge_{O\text{-}O}$ (a.u.)	$Spin_{O\text{-}O}$ (a.u.) (a.u.)
Anions	1-3-G-T	1.45	1.329	−0.720	0.986
	3-3-G-T	0.77	1.321	−0.626	1.038
Cations	1-3-G-Quint	0.78	1.207	+0.129	1.937
	2-3-G-D	0.64	1.207	+0.101	1.984
	3-3-G-T	0.56	1.211	+0.080	1.888
	4-3-G-Q	0.53	1.210	+0.076	1.901
	5-3-G-T	0.51	1.212	+0.061	1.928
	1-4-G-Quint	0.60	1.207	+0.096	1.896
Neutrals	1-3-G-Q	0.39	1.225	−0.065	1.670
	2-3-G-T	0.38	1.225	−0.071	1.729
	4-3-a-T	0.36	1.226	−0.099	1.732

In Figure 4a,b, we summarized the variations of the adsorption energies (E_a) and the stretching frequencies of the adsorbed O_2 vs. the NPA charges localized on the Au atom of the -O-Au sites in $Au_{1-5}O_x^{-/+/0}$ (x = 1 and 2). The considered structures include the lowest-lying ones shown in Figures 1–3 as well as other examples shown in Figures S1–S12. For anionic $Au_{1-5}O_x^-$ (x = 1 and 2), a roughly inverse correlation was observed between the adsorption energies (E_a) and the NPA charges. The E_a values decrease from around 1.5 eV to around 0.5 eV when the NPA charges increase from around −0.1 a.u. to around +0.4 a.u. The stretching frequencies of the adsorbed O_2 on the -O-Au sites concentrate in the range of 1100 to 1200 cm^{-1}. These values are much lower than the calculated stretching frequencies of a free O_2, which stands at 1637 cm^{-1} (1580 cm^{-1} as reported in experiment [74]), and there is not a clear correlation between these frequencies and the NPA charges. For cationic gold oxide clusters $Au_{1-5}O_x^+$ (x = 1 and 2), an approximately positive correlation exists between the E_a values and the NPA charges on the Au atoms of -O-Au sites. The E_a values increase from around 0.4 eV to around 0.8 eV when the NPA charges increase from around +0.6 a.u. to around +1.0 a.u. The stretching frequencies of the adsorbed O_2 on the -O-Au sites concentrate in the range of 1500 to 1600 cm^{-1}. These values are very close to that of a free O_2, and there is not a clear correlation between these frequencies and the NPA charges. For neutral $Au_{1-5}O_x$ (x = 1 and 2), the adsorption energies (E_a) concentrate around 0.4 eV, which is lower than the E_a values of the anionic and cationic $Au_{1-5}O_x^{-/+}$ (x = 1 and 2). The correlation between E_a and NPA charges of neutral $Au_{1-5}O_x$ (x = 1 and 2) can be viewed as an extension of the positive correlation of cationic $Au_{1-5}O_x^+$ (x = 1 and 2) toward the small NPA charge values. The stretching frequencies of the adsorbed O_2 on the -O-Au sites in neutral clusters spread from 1300 cm^{-1} to 1500 cm^{-1}, which is between the values of the anionic and cationic species.

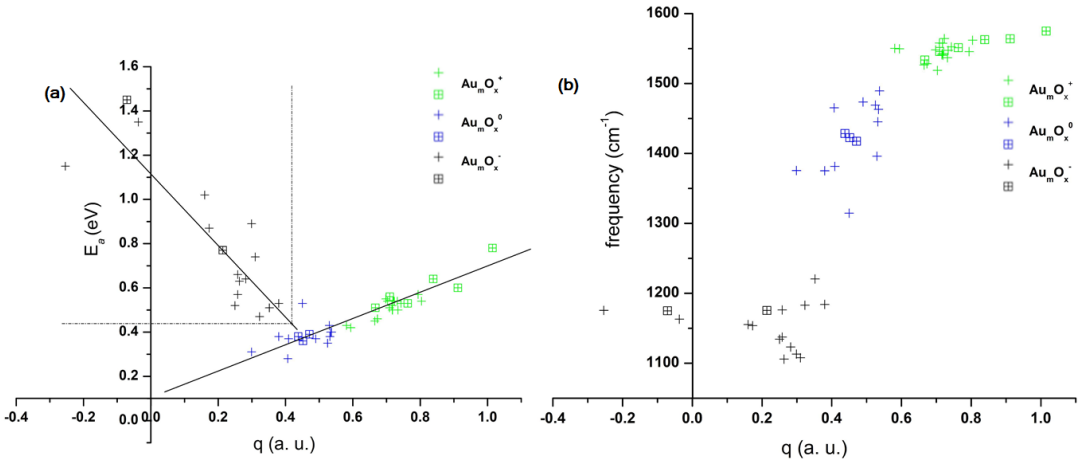

Figure 4. (**a**) The correlations between the adsorption energies (E_a) of O_2 and the NPA charges localized on the Au atoms of -O-Au sites and (**b**) the correlations between the frequencies (cm^{-1}) of the adsorbed O_2 and the NPA charges localized on the Au atoms of the -O-Au sites. The data are those of the lowest-lying structures of $Au_{1-5}O_x^{-/+/0}$ (x = 1 and 2) shown in Figures 1–3 (the square symbols ⊞) and other structures (the cross symbols +) with the -O-Au sites in the Supplementary Materials. The results of the anionic, the neutral, and the cationic species are shown by the black, the blue, and the green symbols, respectively.

2.5. Analyses on the Bonding Patterns

In order to understand the charge-dependent bonding strengths and activation degrees of O_2 on the -O-Au sites of various clusters, we conducted an analysis of the density of states (DOSs). This analysis allowed us to identify the bonding patterns in several representative structures with differing charge polarities. The density of states (DOSs) of AuO^- (1-1-G-S), AuO^+ (1-1-G-T), AuO (1-1-G-D), Au_3O^- (3-1-G-S), Au_3O^+ (3-1-c-T), and Au_3O (3-1-a-D) are shown in Figure 5a,c,e,g,i,k, respectively. The density of states (DOSs) of their adsorption products, AuO_3^- (1-3-G-T), AuO_3^+ (1-3-G-Quint), AuO_3 (1-3-G-Q), $Au_3O_3^-$ (3-3-G-T), $Au_3O_3^+$ (3-3-b-Quint), and Au_3O_3 (3-3-G-Q), and the partial density of states (PDOSs) of the adsorbed O_2 are shown in Figure 5b,d,f,h,j,l, respectively.

Insights from the results of AuO^- (1-1-G-S), AuO_3^- (1-3-G-T), Au_3O^- (3-1-G-S), and $Au_3O_3^-$ (3-3-G-T) presented in Figure 5a,b,g,h, reveal that the two up-spin and one down-spin components originating from the π_{2p}* of O_2 are occupied in the adsorption products. These observations suggest that a single electron has been transferred from the anionic gold oxide clusters to the adsorbed O_2, which follows a pattern reminiscent of O_2 adsorption on active Au_n^- [51]. It is crucial to note that an excess electron on the π_{2p}* of O_2 may substantially weaken the O-O bond strength, echoing the findings shown in Table 1 and Figure 4. The interaction process between AuO^- (1-1-G-S) or Au_3O^- (3-1-G-S) and O_2 can be elaborated as follows: an electron located on one HOMO ($\pi^*_{//}$) of the anionic cluster is excited to its LUMO (the σ orbital enclosed by a blue frame). Consequently, the occupied σ orbital, which extends externally, showcases a high propensity for σ bond formation. Subsequently, the interaction between this σ orbital and one singly occupied π* orbital of O_2, results in an occupied σ orbital and an unoccupied σ orbital. This newly formed occupied σ orbital boasts bonding characters predominantly comprised of the π* orbital of O_2, and the newly formed unoccupied σ orbital exhibits antibonding characters mainly originating from the LUMO of AuO^- or Au_3O^-. These chemical bonding figures can account for the strong bonding strengths and the high activation degrees of O_2 in these anionic species.

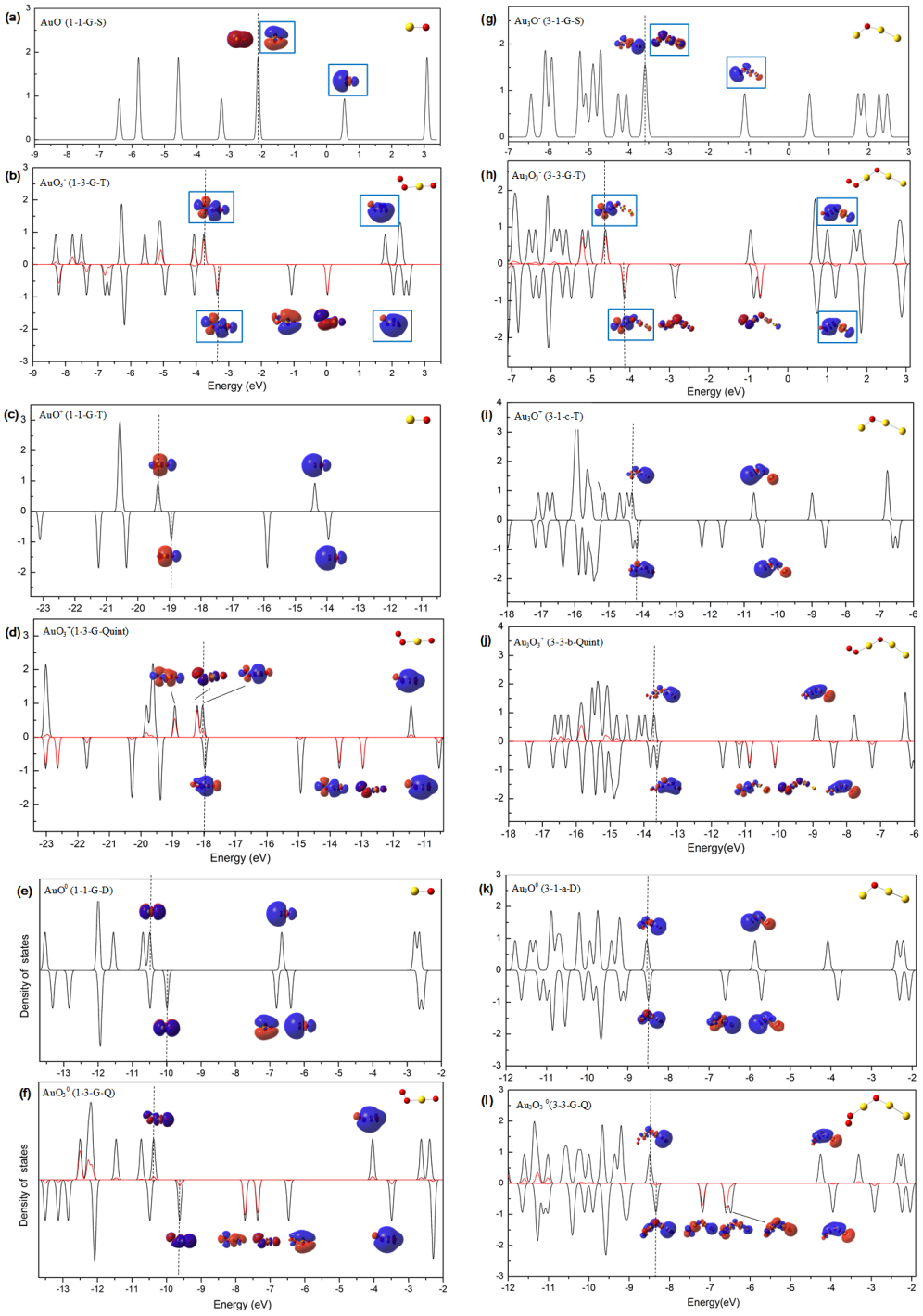

Figure 5. The DOS and PDOS (O_2) figures in (**a**) AuO^- (1-1-G-S) and (**b**) AuO_3^- (1-3-G-T); (**c**) AuO^+ (1-1-G-T) and (**d**) AuO_3^+ (1-3-G-Quint); (**e**) AuO (1-1-G-D) and (**f**) AuO_3 (1-3-G-Q); (**g**) Au_3O^- (3-1-G-S) and (**h**) $Au_3O_3^-$ (3-3-G-T); (**i**) Au_3O^+ (3-1-c-T) and (**j**) $Au_3O_3^+$ (3-3-b-Quint); (**k**) Au_3O (3-1-a-D) and (**l**) Au_3O_3 (3-3-G-Q). In each panel, the DOSs and PDOSs (O_2) are plotted in black and in red, respectively; the HOMO position is indicated by a dotted line. The figures of some orbitals (those around the HOMO position) are shown to illustrate the bonding interactions between the gold oxide clusters and O_2, and the orbitals enclosed by blue frames stand for the ones most correlated with these interactions. These results were obtained according to the KS orbitals from the calculations at the B3LYP level with the basis sets of def2-SVP for Au and def2-TZVP for O.

According to the calculated DOSs of AuO^+ (1-1-G-T), AuO_3^+ (1-3-G-Quint), Au_3O^- (3-1-c-T), and $Au_3O_3^+$ (3-3-b-Quint) shown in Figure 5c,d,i,j, the up-spin and down-spin components on the cluster moiety and the O_2 do not apparently change during the adsorption reactions, and marginal electron transfer can be distinguished. The bonding interaction between the two moieties could be related to mixing of the filled up-spin components of gold oxide and the filled up-spin π^* components of O_2. For the corresponding neutral examples, AuO (1-1-G-D), AuO_3 (1-3-G-Q), Au_3O (3-1-a-D), and Au_3O_3 (3-3-G-Q), their calculated DOSs shown in Figure 5e,f,k,l, present scenarios similar to those of cations. The main contributions to the bonding interactions in these cationic and neutral species can be attributed to electrostatic attractions between the more or less positively charged Au atom of -O-Au sites and the polarized O_2 molecule. The more positively charged Au atom of -O-Au sites in the cationic gold oxide clusters can interpret their marginally stronger bonding strengths with O_2 than those in the neutral ones. At the same time, the more positively charged Au atom of -O-Au sites can more effectively prevent electron transfer to the π^* orbital of O_2 and therefore lead to the lower activation degrees of O_2 in the cationic ones.

3. Methods

The structures of $Au_{1–5}O_x^{-/+/0}$ (x = 1–4) were preliminarily identified using a modified version of the Deaven–Ho genetic algorithm [35,75–77]. The modification involved incorporating incomplete optimizations of descendant structures from each crossover and mutation step [78]. The reliability, feasibility, and efficiency of this algorithmic procedure have been demonstrated in our previous published articles [64,78,79].

The specific implementation process is as follows:

(1) In our search program, we specify the number of gold and oxygen atoms and the multiplicity of the clusters. Based on the complexity of cluster searching, we determine the type and number of initial structures as initial random structures with diverse motifs. We have designed a module capable of generating seven typical motifs for a defined cluster size: the space-free motif, the close packing motif, the simple cubic packing motif, the cage motif, the solid sphere motif, the ring motif, and the specially defined motif through atomic coordinates. The latter allows users to input specially defined or previously reported structures.

(2) The initial random structures undergo relaxation using an incomplete optimization approach and are screened using the competition method under the small basis set we specify. The surviving structures become the offspring of the first generation.

(3) The first-generation results undergo multiple iterations of crossover and mutation under the genetic algorithm framework, generating a substantial number of offspring. After deduplication and competition, the next generation of structures is produced. This cycle continues until a global minimum is attained under the specified convergence limit. The structure optimizations at this stage were performed using a relatively coarse DFT method. Specifically, the B3LYP hybrid functional [80,81] with the LANL2DZ basis set [82] for Au and the 6–31+G* basis set [83–85] for O were utilized. For each $Au_{1–5}O_x^{-/+/0}$ (x = 1–2), the program explored structure candidates in the two lowest-lying spin multiplicities, and for each $Au_{1–5}O_x^{-/+/0}$ (x = 3–4), the program explored structure candidates in the three lowest-lying spin multiplicities. When conducting a structural search for the system containing three to four O atoms, the randomly generated structures consist of either all the O atoms being randomly dispersed or two of the O atoms combined as an O_2 unit being adsorbed on the remaining gold oxide clusters containing a single O atom or two O atoms.

(4) All structures that were relatively stable (within approximately 1.0 eV of the lowest-lying one) underwent further optimization and scrutiny at a more sophisticated theory level, in which the B3LYP hybrid functional in combination with the def2-SVP basis set for Au and the def2-TZVP basis sets for O [86,87] was utilized. Scalar and spin-orbital relativistic effects of Au were addressed through energy consistent relativistic

pseudopotentials. The ultimate global minima were validated via vibrational mode analysis, confirming the absence of imaginary frequencies.

(5) The adsorption energies of O_2 on specific structures were calculated based on the Hartree–Fock energies corrected by the zero-point energies from frequency analyses. The formula for calculating the adsorption energy is the sum of the energies of the gold oxide cluster and O_2, minus the energy of the compound after adsorption. The distribution of charges localized on the adsorbed O_2 and the Au atom of the -O-Au sites were examined using the Natural Bond Analysis method [88]. The density of state (DOS) spectrum was obtained by broadening the calculated Kohn–Sham (KS) orbitals from the more sophisticated theory level using the Gaussian function with a FWHM of 0.1 eV. The position of HOMO in the DOS spectrum has been corrected using the clusters' vertical detachment energy (VDE) values. All DFT calculations were performed using the Gaussian 09 program [89], and the DOS spectra were generated from the calculation results using the Multiwfn software [90].

4. Conclusions

Using an improved genetic algorithm program combined with DFT methods, we conducted extensive calculations on the structures of $Au_{1–5}O_{1,2}{}^{-/+/0}$ and their corresponding products after adsorbing an O_2, $Au_{1–5}O_{3,4}{}^{-/+/0}$. The preferred adsorption sites and the charge-dependence of the adsorption strengths and the activation degrees were analyzed. The conclusions are as follow:

1. Regardless of the charge states of gold oxide clusters, the -O-Au sites are inevitably the primary sites for O_2 adsorption.
2. The charge states of gold oxide clusters determine the bonding strengths and the activation degrees of the adsorbed O_2. For anionic gold oxide clusters, the occurrence of electron transfer from the -O-Au sites to the adsorbed O_2 leads to the formation of typical chemical bonds and high activation degrees of O_2. For both cationic and neutral gold oxide clusters, their interactions with O_2 are predominantly electrostatic. More positive charges on the Au atom of -O-Au sites in the cationic clusters lead to stronger binding energies than those of corresponding neutral ones. Meanwhile, the lower electron densities around the Au atom of -O-Au sites in the cationic clusters make electron transfer to O_2 more unlikely, and O_2 activation on the cationic gold oxide clusters is less effective than those in neutral species.

These findings could deepen the understanding of intricate charge effects on the ability of active sites on gold-based catalysts to activate O_2 and offer pivotal information to reveal their catalytic mechanisms at the atomic and molecular level.

Supplementary Materials: The following supporting information can be downloaded at: https://www.mdpi.com/article/10.3390/molecules29071645/s1, Figure S1: Low-lying structures of $Au_{1-2}O_x{}^-$ (x = 1–4). Figure S2: Low-lying structures of $Au_3O_x{}^-$ (x = 1–4). Figure S3: Low-lying structures of $Au_4O_x{}^-$ (x = 1–4). Figure S4: Low-lying structures of $Au_5O_x{}^-$ (x = 1–4). Figure S5: Low-lying structures of $Au_{1-2}O_x{}^+$ (x = 1–4). Figure S6: Low-lying structures of $Au_3O_x{}^+$ (x = 1–4). Figure S7: Low-lying structures of $Au_4O_x{}^+$ (x = 1–4). Figure S8: Low-lying structures of $Au_5O_x{}^+$ (x = 1–4). Figure S9: Low-lying structures of $Au_{1-2}O_x$ (x = 1–4). Figure S10: Low-lying structures of Au_3O_x (x = 1–4). Figure S11: Low-lying structures of Au_4O_x (x = 1–4). Figure S12: Low-lying structures of Au_5O_x (x = 1–4).

Author Contributions: Conceptualization, L.H. and X.X.; methodology, L.H.; software, W.L.; validation, X.X. and L.H.; investigation, L.H.; writing—original draft preparation, X.X. and L.H.; writing—review and editing, X.X. and L.H.; visualization, L.H.; supervision, X.X.; funding acquisition, X.X. All authors have read and agreed to the published version of the manuscript.

Funding: This work was supported by the National Natural Science Foundation of China (Grant No. 22273065, 21673158) and the Science and Technology Commission of Shanghai Municipality (14DZ2261100).

Institutional Review Board Statement: Not applicable.

Informed Consent Statement: Not applicable.

Data Availability Statement: Data are contained within the article and Supplementary Materials.

Acknowledgments: The theoretical calculations were carried out using the computing resource in the National Supercomputing Center in Shenzhen.

Conflicts of Interest: The authors declare no conflicts of interest.

References

1. Bell, A.T. The Impact of Nanoscience on Heterogeneous Catalysis. *Science* **2003**, *299*, 1688–1691. [CrossRef] [PubMed]
2. Besson, M.; Gallezot, P.; Pinel, C. Conversion of Biomass into Chemicals over Metal Catalysts. *Chem. Rev.* **2014**, *114*, 1827–1870. [CrossRef] [PubMed]
3. Pacchioni, G.; Freund, H.-J. Controlling the Charge State of Supported Nanoparticles in Catalysis: Lessons from Model Systems. *Chem. Soc. Rev.* **2018**, *47*, 8474–8502. [CrossRef] [PubMed]
4. Lou, Y.; Xu, J.; Zhang, Y.; Pan, C.; Dong, Y.; Zhu, Y. Metal-support Interaction for Heterogeneous Catalysis: From Nanoparticles to Single Atoms. *Mater. Today Nano* **2020**, *12*, 100093. [CrossRef]
5. Liu, L.; Corma, A. Metal Catalysts for Heterogeneous Catalysis: From Single Atoms to Nanoclusters and Nanoparticles. *Chem. Rev.* **2018**, *118*, 4981–5079. [CrossRef]
6. van Deelen, T.W.; Mejia, C.H.; de Jong, K.P. Control of Metal-support Interactions in Heterogeneous Catalysts to Enhance Activity and Selectivity. *Nat. Catal.* **2019**, *2*, 955–970. [CrossRef]
7. Haruta, M.; Yamada, N.; Kobayashi, T.; Iijima, S. Gold Catalysts Prepared by Coprecipitation for Low-temperature Oxidation of Hydrogen and of Carbon Monoxide. *J. Catal.* **1989**, *115*, 301–309. [CrossRef]
8. Haruta, M. Size- and Support-dependency in the Catalysis of Gold. *Catal. Today* **1997**, *36*, 153–166. [CrossRef]
9. Cunningham, D.A.H.; Vogel, W.; Kageyama, H.; Tsubota, S.; Haruta, M. The Relationship between the Structure and Activity of Nanometer Size Gold When Supported on $Mg(OH)_2$. *J. Catal.* **1998**, *177*, 1–10. [CrossRef]
10. Blick, K.; Mitrelias, T.D.; Hargreaves, J.S.J.; Hutchings, G.J.; Joyner, R.W.; Kiely, C.J.; Wagner, F.E. Methane Oxidation Using Au/MgO Catalysts. *Catal. Lett.* **1998**, *50*, 211–218. [CrossRef]
11. Finch, R.M.; Hodge, N.A.; Hutchings, G.J.; Meagher, A.; Pankhurst, Q.A.; Siddiqui, M.R.H.; Wagner, F.E.; Whyman, R. Identification of Active Phases in Au-Fe Catalysts for Low-temperature CO Oxidation. *Phys. Chem. Chem. Phys.* **1999**, *1*, 485–489. [CrossRef]
12. Widmann, D.; Behm, R.J. Activation of Molecular Oxygen and the Nature of the Active Oxygen Species for CO Oxidation on Oxide Supported Au Catalysts. *Acc. Chem. Res.* **2014**, *47*, 740–749. [CrossRef] [PubMed]
13. Montemore, M.M.; van Spronsen, M.A.; Madix, R.J.; Friend, C.M. O_2 Activation by Metal Surfaces: Implications for Bonding and Reactivity on Heterogeneous Catalysts. *Chem. Rev.* **2018**, *118*, 2816–2862. [CrossRef] [PubMed]
14. Staykov, A.; Miwa, T.; Yoshizawa, K. Aerobic Oxidation of Alkanes on Icosahedron Gold Nanoparticle Au_{55}. *J. Catal.* **2018**, *364*, 141–153. [CrossRef]
15. Ke, Y.; Li, X.; Li, J.; Liu, C.-L.; Xu, C.; Dong, W.-S. Conversion of Glycerol to Dihydroxyacetone over Au Catalysts on Various Supports. *J. Chem. Technol. Biotechnol.* **2020**, *95*, 1153–1162. [CrossRef]
16. Shcherbakov, V.; Denisov, S.A.; Mostafavi, M. Selective Oxidation of Transient Organic Radicals in the Presence of Gold Nanoparticles. *Nanomaterials* **2021**, *11*, 727. [CrossRef] [PubMed]
17. Deka, R.C.; Bhattacharjee, D.; Chakrabartty, A.K.; Mishra, B.K. Catalytic Oxidation of NO by Au_2^- Dimers: A DFT Study. *Rsc. Adv.* **2014**, *4*, 5399–5404. [CrossRef]
18. Pal, R.; Wang, L.M.; Pei, Y.; Wang, L.S.; Zeng, X.C. Unraveling the Mechanisms of O_2 Activation by Size-selected Gold Clusters: Transition from Superoxo To Peroxo Chemisorption. *J. Am. Chem. Soc.* **2012**, *134*, 9438–9445. [CrossRef] [PubMed]
19. Fujita, T.; Guan, P.; McKenna, K.; Lang, X.; Hirata, A.; Zhang, L.; Tokunaga, T.; Arai, S.; Yamamoto, Y.; Tanaka, N.; et al. Atomic Origins of the High Catalytic Activity of Nanoporous Gold. *Nat. Mater.* **2012**, *11*, 775–780. [CrossRef]
20. Roldan, A.; Manel Ricart, J.; Illas, F.; Pacchioni, G. O_2 Adsorption and Dissociation on Neutral, Positively and Negatively Charged Au_n(n = 5–79) Clusters. *Phys. Chem. Chem. Phys.* **2010**, *12*, 10723–10729. [CrossRef]
21. Woodham, A.P.; Fielicke, A. Superoxide Formation on Isolated Cationic Gold Clusters. *Angew. Chem. Int. Ed.* **2014**, *53*, 6554–6557. [CrossRef] [PubMed]
22. Turner, M.; Golovko, V.B.; Vaughan, O.P.H.; Abdulkin, P.; Berenguer-Murcia, A.; Tikhov, M.S.; Johnson, B.F.G.; Lambert, R.M. Selective Oxidation with Dioxygen by Gold Nanoparticle Catalysts Derived from 55-atom Clusters. *Nature* **2008**, *454*, 981–984. [CrossRef] [PubMed]
23. Pacchioni, G. Electronic Interactions and Charge Transfers of Metal Atoms and Clusters on Oxide Surfaces. *Phys. Chem. Chem. Phys.* **2013**, *15*, 1737–1757. [CrossRef] [PubMed]
24. Lang, S.M.; Bernhardt, T.M.; Barnett, R.N.; Landman, U. Temperature-Tunable Selective Methane Catalysis on Au_2^+: From Cryogenic Partial Oxidation Yielding Formaldehyde to Cold Ethylene Production. *J. Phys. Chem. C* **2011**, *115*, 6788–6795. [CrossRef]

25. Yuan, Z.; Li, X.-N.; He, S.-G. CO Oxidation Promoted by Gold Atoms Loosely Attached in $AuFeO_3^-$ Cluster Anions. *J. Phys. Chem. Lett.* **2014**, *5*, 1585–1590. [CrossRef]
26. Baishya, S.; Deka, R.C. Catalytic Activities of Au_6, Au_6^-, and Au_6^+ Clusters for CO Oxidation: A Density Functional Study. *Int. J. Quantum. Chem.* **2014**, *114*, 1559–1566. [CrossRef]
27. Woodham, A.P.; Meijer, G.; Fielicke, A. Charge Separation Promoted Activation of Molecular Oxygen by Neutral Gold Clusters. *J. Am. Chem. Soc.* **2013**, *135*, 1727–1730. [CrossRef]
28. Zhou, X.; Shen, Q.; Yuan, K.; Yang, W.; Chen, Q.; Geng, Z.; Zhang, J.; Shao, X.; Chen, W.; Xu, G.; et al. Unraveling Charge State of Supported Au Single-Atoms during CO Oxidation. *J. Am. Chem. Soc.* **2018**, *140*, 554–557. [CrossRef]
29. Camellone, M.F.; Fabris, S. Reaction Mechanisms for the CO Oxidation on Au/CeO_2 Catalysts: Activity of Substitutional Au_3^+/Au^+ Cations and Deactivation of Supported Au^+ Adatoms. *J. Am. Chem. Soc.* **2009**, *131*, 10473–10483. [CrossRef]
30. Yoon, B.; Hakkinen, H.; Landman, U.; Worz, A.S.; Antonietti, J.M.; Abbet, S.; Judai, K.; Heiz, U. Charging Effects on Bonding and Catalyzed Oxidation of CO on Au_8 Clusters on MgO. *Science* **2005**, *307*, 403–407. [CrossRef]
31. Burgel, C.; Reilly, N.M.; Johnson, G.E.; Mitric, R.; Kimble, M.L.; Castleman, A.W., Jr.; Bonacic-Koutecky, V. Influence of Charge State on the Mechanism of CO Oxidation on Gold Clusters. *J. Am. Chem. Soc.* **2008**, *130*, 1694–1698. [CrossRef] [PubMed]
32. Min, B.K.; Friend, C.M. Heterogeneous Gold-based Catalysis for Green Chemistry: Low-temperature CO Oxidation and Propene Oxidation. *Chem. Rev.* **2007**, *107*, 2709–2724. [CrossRef] [PubMed]
33. Jeong, E.; Choi, E.-A.; Ikoma, Y.; Yu, S.M.; Bae, J.-S.; Lee, S.-G.; Han, S.Z.; Lee, G.-H.; Yun, J. An Unexpected Role of Atomic Oxygen Dopants in Au Evolution from Clusters to A Layer. *Acta Mater.* **2021**, *202*, 277–289. [CrossRef]
34. Li, Y.; Dononelli, W.; Moreira, R.; Risse, T.; Baeumer, M.; Kluener, T.; Moskaleva, L.V. Oxygen-Driven Surface Evolution of Nanoporous Gold: Insights from Ab Initio Molecular Dynamics and Auger Electron Spectroscopy. *J. Phys. Chem. C* **2018**, *122*, 5349–5357. [CrossRef]
35. Baber, A.E.; Torres, D.; Muller, K.; Nazzarro, M.; Liu, P.; Starr, D.E.; Stacchiola, D.J. Reactivity and Morphology of Oxygen-Modified Au Surfaces. *J. Phys. Chem. C* **2012**, *116*, 18292–18299. [CrossRef]
36. Xu, B.; Haubrich, J.; Baker, T.A.; Kaxiras, E.; Friend, C.M. Theoretical Study of O-Assisted Selective Coupling of Methanol on Au(111). *J. Phys. Chem. C* **2011**, *115*, 3703–3708. [CrossRef]
37. Alves, L.; Ballesteros, B.; Boronat, M.; Cabrero-Antonino, J.R.; Concepcion, P.; Corma, A.; Correa-Duarte, M.A.; Mendoza, E. Synthesis and Stabilization of Subnanometric Gold Oxide Nanoparticles on Multiwalled Carbon Nanotubes and Their Catalytic Activity. *J. Am. Chem. Soc.* **2011**, *133*, 10251–10261. [CrossRef] [PubMed]
38. Biener, J.; Biener, M.M.; Nowitzki, T.; Hamza, A.V.; Friend, C.M.; Zielasek, V.; Baeumer, M. On the Role of Oxygen in Stabilizing Low-coordinated Au Atoms. *Chemphyschem* **2006**, *7*, 1906–1908. [CrossRef] [PubMed]
39. Baker, T.A.; Liu, X.; Friend, C.M. The mystery of gold's chemical activity: Local bonding, morphology and reactivity of atomic oxygen. *Phys. Chem. Chem. Phys.* **2011**, *13*, 34–46. [CrossRef]
40. Qin, R.; Liu, K.; Wu, Q.; Zheng, N. Surface Coordination Chemistry of Atomically Dispersed Metal Catalysts. *Chem. Rev.* **2020**, *120*, 11810–11899. [CrossRef]
41. Zhou, Y.; Perket, J.M.; Zhou, J. Growth of Pt Nanoparticles on Reducible CeO_2 (111) Thin Films: Effect of Nanostructures and Redox Properties of Ceria. *J. Phys. Chem. C* **2010**, *114*, 11853–11860. [CrossRef]
42. Tanaka, H.; Neukermans, S.; Janssens, E.; Silverans, R.E.; Lievens, P. Sigma Aromaticity of the Bimetallic Au_5Zn^+ Cluster. *J. Am. Chem. Soc.* **2003**, *125*, 2862–2863. [CrossRef]
43. Sergeeva, A.P.; Popov, I.A.; Piazza, Z.A.; Li, W.-L.; Romanescu, C.; Wang, L.-S.; Boldyrev, A.I. Understanding Boron through Size-Selected Clusters: Structure, Chemical Bonding, and Fluxionality. *Acc. Chem. Res.* **2014**, *47*, 1349–1358. [CrossRef] [PubMed]
44. Li, X.; Kiran, B.; Cui, L.F.; Wang, L.S. Magnetic Properties in Transition-metal-doped Gold Clusters: $M@Au_6$ (M = Ti, V, Cr). *Phys. Rev. Lett.* **2005**, *95*, 253401. [CrossRef] [PubMed]
45. Lang, S.M.; Bernhardt, T.M. Gas Phase Metal Cluster Model Systems for Heterogeneous Catalysis. *Phys. Chem. Chem. Phys.* **2012**, *14*, 9255–9269. [CrossRef] [PubMed]
46. Wang, T.; Ma, J.; Yin, B.; Xing, X. Adsorption of O_2 on Anionic Gold Clusters in the 0–1 nm Size Range: An Insight into the Electron Transfer Dynamics from Kinetic Measurements. *J. Phys. Chem. A* **2018**, *122*, 3346–3352. [CrossRef]
47. Salisbury, B.E.; Wallace, W.T.; Whetten, R.L. Low-temperature Activation of Molecular Oxygen by Gold Clusters: A Stoichiometric Process Correlated to Electron Affinity. *Chem. Phys.* **2000**, *262*, 131–141. [CrossRef]
48. Huang, W.; Zhai, H.-J.; Wang, L.-S. Probing the Interactions of O_2 with Small Gold Cluster Anions (Au_n^-, n = 1–7): Chemisorption *vs* Physisorption. *J. Am. Chem. Soc.* **2010**, *132*, 4344–4351. [CrossRef]
49. Woodham, A.P.; Meijer, G.; Fielicke, A. Activation of Molecular Oxygen by Anionic Gold Clusters. *Angew. Chem. Int. Ed. Engl.* **2012**, *51*, 4444–4447. [CrossRef]
50. Mills, G.; Gordon, M.S.; Metiu, H. The Adsorption of Molecular Oxygen on Neutral and Negative Au_nClusters (n = 2–5). *Chem. Phys. Lett.* **2002**, *359*, 493–499. [CrossRef]
51. Yoon, B.; Hakkinen, H.; Landman, U. Interaction of O_2 with Gold Clusters: Molecular and Dissociative Adsorption. *J. Phys. Chem. A* **2003**, *107*, 4066–4071. [CrossRef]
52. Sun, Q.; Jena, P.; Kim, Y.D.; Fischer, M.; Gantefor, G. Interactions of Au Cluster Anions with Oxygen. *J. Chem. Phys.* **2004**, *120*, 6510–6515. [CrossRef] [PubMed]

53. Lee, H.M.; Lee, K.H.; Lee, G.; Kim, K.S. Geometrical and Electronic Characteristics of $Au_nO_2^-$ (n = 2–7). *J. Phys. Chem. C* **2015**, *119*, 14383–14391. [CrossRef]
54. Okumura, M.; Kitagawa, Y.; Haruta, M.; Yamaguchi, K. DFT Studies of Interaction between O_2 and Au Clusters. The Role of Anionic Surface Au Atoms on Au Clusters for Catalyzed Oxygenation. *Chem. Phys. Lett.* **2001**, *346*, 163–168. [CrossRef]
55. Shi, H.X.; Sun, W.G.; Kuang, X.Y.; Lu, C.; Xia, X.X.; Chen, B.L.; Hermann, A. Probing the Interactions of O_2 with Small Gold Cluster Au_n^Q (n = 2–10, Q = 0, −1): A Neutral Chemisorbed Complex Au_5O_2 Cluster Predicted. *J. Phys. Chem. C* **2017**, *121*, 24886–24893. [CrossRef]
56. Ding, X.-L.; Liao, H.-L.; Zhang, Y.; Chen, Y.-M.; Wang, D.; Wang, Y.-Y.; Zhang, H.-Y. Geometric and Electronic Properties of Gold Clusters Doped with A Single Oxygen Atom. *Phys. Chem. Chem. Phys.* **2016**, *18*, 28960–28972. [CrossRef]
57. Zhai, H.-J.; Buergel, C.; Bonacic-Koutecky, V.; Wang, L.-S. Probing the Electronic Structure and Chemical Bonding of Gold Oxides and Sulfides in AuO_n^- and AuS_n^- (n = 1, 2). *J. Am. Chem. Soc.* **2008**, *130*, 9156–9167. [CrossRef]
58. Kimble, M.L.; Castleman, A.W. Gas-phase Studies of $Au_nO_m^+$ Interacting with Carbon Monoxide. *Int. J. Mass Spectrom.* **2004**, *233*, 99–101. [CrossRef]
59. Kimble, M.L.; Castleman, A.W.; Mitric, R.; Burgel, C.; Bonacic-Koutecky, V. Reactivity of Atomic Gold Anions toward Oxygen and the Oxidation of CO: Experiment and Theory. *J. Am. Chem. Soc.* **2004**, *126*, 2526–2535. [CrossRef]
60. Kimble, M.L.; Castleman, A.W.; Bürgel, C.; Bonačić-Koutecký, V. Interactions of CO with $Au_nO_m^-$ ($n \geq 4$). *Int. J. Mass Spectrom.* **2006**, *254*, 163–167. [CrossRef]
61. Kimble, M.L.; Moore, N.A.; Johnson, G.E.; Castleman, A.W.; Burgel, C.; Mitric, R.; Bonacic-Koutecky, V. Joint Experimental and Theoretical Investigations of the Reactivity of $Au_2O_n^-$ and $Au_3O_n^-$ (n = 1–5) with Carbon Monoxide. *J. Chem. Phys.* **2006**, *125*, 240311. [CrossRef] [PubMed]
62. Kimble, M.L.; Moore, N.A.; Castleman, A.W., Jr.; Buergel, C.; Mitric, R.; Bonacic-Koutecky, V. Reactivity of Anionic Gold Oxide Clusters Towards CO: Experiment and Theory. *Eur. Phys. J. D.* **2007**, *43*, 205–208. [CrossRef]
63. Yin, B.; Wang, T.; Chen, Y.; Yang, J.; Wang, G.; Xing, X. Cooperative Bonding Interactions of Various Oxygen Species on the IB Group Metal Anions. *Int. J. Mass Spectrom.* **2020**, *451*, 116312. [CrossRef]
64. Huang, L.; Liu, W.; Hu, J.; Xing, X. Adsorption and Activation of O_2 on Small Gold Oxide Clusters: The Reactivity Dominated by Site-Specific Factors. *J. Phys. Chem. A* **2022**, *126*, 5594–5603. [CrossRef] [PubMed]
65. Ricci, D.; Bongiorno, A.; Pacchioni, G.; Landman, U. Bonding Trends and Dimensionality Crossover of Gold Nanoclusters on Metal-Supported MgO Thin Films. *Phys. Rev. Lett.* **2006**, *97*, 036106. [CrossRef]
66. Mäkinen, M.; Laasonen, K. Density Functional Theory Study of Trends in Water Dissociation on Oxygen-preadsorbed and Pure Transition Metal Surfaces. *Sur. Sci.* **2023**, *734*, 122305. [CrossRef]
67. Liu, X.; Yang, J.; Shen, G.; Shen, M.; Zhao, Y.; Cho, K.; Shan, B.; Chen, R. Tuning the Structure of Bifunctional $Pt/SmMn_2O_5$ Interfaces for Promoted Low-temperature CO oxidation Activity. *Nanoscale* **2019**, *11*, 8150–8159. [CrossRef]
68. Savchenko, V.I.; Boreskov, G.K.; Kalinkin, A.V.; Salanov, A.N. State of Oxygen on Metal Surfaces and Catalytic Activity for the Oxidation of Carbon Monoxide. *Kinet. Catal.* **1983**, *24*, 1154–1161.
69. Liao, M.-S.; Watts, J.D.; Huang, M.-J. Theoretical Comparative Study of Oxygen Adsorption on Neutral and Anionic $Ag_n$and Au_nClusters (n = 2–25). *J. Phys. Chem. C* **2014**, *118*, 21911–21927. [CrossRef]
70. Ding, X.; Li, Z.; Yang, J.; Hou, J.G.; Zhu, Q. Adsorption Energies of Molecular Oxygen on Au Clusters. *J. Chem. Phys.* **2004**, *120*, 9594–9600. [CrossRef]
71. Ferrari, P.; Janssens, E. Argon Adsorption on Cationic Gold Clusters Au_n^+ ($n \leq 20$). *Molecules* **2021**, *26*, 4082. [CrossRef] [PubMed]
72. Ferrari, P.; Hou, G.-L.; Lushchikova, O.V.; Calvo, F.; Bakker, J.M.; Janssens, E. The Structures of Cationic Gold Clusters Probed by Far-infrared Spectroscopy. *Phys. Chem. Chem. Phys.* **2020**, *22*, 11572–11577. [CrossRef] [PubMed]
73. Ferrari, P.; Hussein, H.A.; Heard, C.J.; Vanbuel, J.; Johnston, R.L.; Lievens, P.; Janssens, E. Effect of Palladium Doping on the Stability and Fragmentation Patterns of Cationic Gold Clusters. *Phys. Rev. A* **2018**, *97*, 052508. [CrossRef]
74. Computational Chemistry Comparison and Benchmark DataBase. Available online: https://cccbdb.nist.gov/exp2x.asp?casno=7782447&charge=0 (accessed on 22 May 2022).
75. Deaven, D.M.; Ho, K.M. Molecular-Geometry Optimization with a Genetic Algorithm. *Phys. Rev. Lett.* **1995**, *75*, 288–291. [CrossRef] [PubMed]
76. Deaven, D.M.; Tit, N.; Morris, J.R.; Ho, K.M. Structural Optimization of Lennard-Jones Clusters by A Genetic Algorithm. *Chem. Phys. Lett.* **1996**, *256*, 195–200. [CrossRef]
77. Stowers, K.J.; Madix, R.J.; Friend, C.M. From Model Studies on Au(111) to Working Conditions with Unsupported Nanoporous Gold Catalysts: Oxygen-assisted Coupling Reactions. *J. Catal.* **2013**, *308*, 131–141. [CrossRef]
78. Liu, W.; Huang, L.; Meng, L.; Hu, J.; Xing, X. The Global Minimum of Ag_{30}: A Prolate Spheroidal Structure Predicted by the Genetic Algorithm with Incomplete Local Optimizations at a DFT Level. *Phys. Chem. Chem. Phys.* **2023**, *25*, 14303–14310. [CrossRef] [PubMed]
79. Huang, L.; Liu, W.; Hu, J.; Xing, X. Exploring the Effects of a Doping Silver Atom on Anionic Gold Clusters' Reactivity with O_2. *J. Phys. Chem. A* **2021**, *125*, 9995–10005. [CrossRef]
80. Becke, A. Becke's Three Parameter Hybrid Method Using the LYP Correlation Functional. *J. Chem. Phys.* **1993**, *98*, 5648. [CrossRef]
81. Lee, C.; Yang, W.; Parr, R.G. Development of the Colle-Salvetti Correlation-energy Formula into a Functional of the Electron Density. *Phys. Rev. B* **1988**, *37*, 785–789. [CrossRef]

82. Hay, P.J.; Wadt, W.R. Abinitio Effective Core Potentials for Molecular Calculations—Potentials for K to Au Including the Outermost Core Orbitals. *J. Chem. Phys.* **1985**, *82*, 299–310. [CrossRef]
83. Krishnan, R.; Binkley, J.S.; Seeger, R.; Pople, J.A. Self-Consistent Molecular-Orbital Methods.20. Basis Set for Correlated Wave-Functions. *J. Chem. Phys.* **1980**, *72*, 650–654. [CrossRef]
84. Hariharan, P.C.; Pople, J.A. The Influence of Polarization Functions on Molecular Orbital Hydrogenation Energies. *Theor. Chim. Acta* **1973**, *28*, 213–222. [CrossRef]
85. Frisch, M.J.; Pople, J.A.; Binkley, J.S. Self-Consistent Molecular-Orbital Methods.25. Supplementary Functions for Gaussian-Basis Sets. *J. Chem. Phys.* **1984**, *80*, 3265–3269. [CrossRef]
86. Schafer, A.; Huber, C.; Ahlrichs, R. Fully Optimized Contracted Gaussian-Basis Sets of Triple Zeta Valence Quality for Atoms Li to Kr. *J. Chem. Phys.* **1994**, *100*, 5829–5835. [CrossRef]
87. Weigend, F.; Ahlrichs, R. Balanced Basis Sets of Split Valence, Triple Zeta V alence and Quadruple Zeta Valence Quality for H to Rn: Design and Assessment of Accuracy. *Phys. Chem. Chem. Phys.* **2005**, *7*, 3297–3305. [CrossRef] [PubMed]
88. Reed, A.E.; Weinstock, R.B.; Weinhold, F. Natural-Population Analysis. *J. Chem. Phys.* **1985**, *83*, 735–746. [CrossRef]
89. Frisch, M.J.; Trucks, G.W.; Schlegel, J.; Scuseria, G.E.; Robb, M.A.; Cheeseman, J.R.; Schlegel, H.B.; Scalmani, G.; Barone, V.; Mennucci, B.; et al. *Gaussian 09, Rev. C.01*; Gaussian, Inc.: Wallingford, CT, USA, 2010.
90. Lu, T.; Chen, F. Multiwfn: A Multifunctional Wavefunction Analyzer. *J. Comput. Chem.* **2012**, *33*, 580–592. [CrossRef]